PCCP

PAPER

View Article Online
View Journal | View Issue

Cite this: *Phys. Chem. Chem. Phys.*, 2018, **20**, 977

Full quantum dynamical investigation of the Eley–Rideal reaction forming H_2 on a movable graphitic substrate at T = 0 K

Marta Pasquini,[a] Matteo Bonfanti [b] and Rocco Martinazzo *[ac]

Received 17th October 2017,
Accepted 6th December 2017

DOI: 10.1039/c7cp07080b

rsc.li/pccp

The dynamics of the Eley–Rideal abstraction reaction of hydrogen atoms on a movable graphitic surface is investigated for the first time in a numerically exact fully quantum setting. A system-bath strategy was applied where the two recombining H atoms and a substrate C atom form a relevant subsystem, while the rest of the lattice takes the form of an independent oscillator bath. High-dimensional wavepacket simulations were performed in the collision energy range 0.2–1.0 eV with the help of the multi-layer multi-configuration time-dependent Hartree method, focusing on the collinear reaction on a zero-temperature surface. Results show that the dynamics is close to a sudden limit in which the reaction is much faster than the substrate motion. Unpuckering of the surface is fast (some tens of fs) but starts only after the formation of H_2 is completed, thereby determining a considerable substrate heating (~0.8 eV per reactive event). Energy partitioning in the product molecule favors translational over vibrational energy, and H_2 molecules are vibrationally hot (~1.5 eV) though to a lesser extent than previously predicted.

1 Introduction

Molecular hydrogen recombination on graphitic surfaces has been widely studied in the last few decades, mainly because of its importance for the physics and the chemistry of the Inter-Stellar Medium (ISM), the rarefied and cold gas which fills the space between stars. H_2 is the most abundant molecular species in the entire Universe: it is involved in most of the reactions occurring in the ISM and plays an important role in the formation of complex chemicals. Moreover, it acts as a radiative cooler during the gravitational collapse of interstellar clouds, the first step in the formation of stars and complex galactic structures.[1] The huge amount of molecular hydrogen requires very efficient formation processes, since H_2 is continuously destroyed under the harsh conditions of the ISM, characterized by intense UV radiation fields and cosmic rays. It is widely believed that H_2 forms on the surface of the interstellar dust grains,[2,3] the 'soot' condensing from the outflows of stars in the asymptotic giant branch. In fact, under typical conditions, gas phase formation pathways are too inefficient to contribute to the H_2 formation rate, except for the early Universe environment where grains had yet to appear. The grains are ~μm-sized particles, and typically consist of a silicate core covered by a mantle whose composition depends on the environment. In the colder, so-called dense clouds icy coatings of H_2O, CO, CO_2 and methanol develop around the grains, while in warmer regions carbon-based, refractory mantles envelop the cores. Furthermore, there exist smaller carbonaceous particles of various sizes – intermediate between grains and molecules, likely polycyclic aromatic hydrocarbons (PAHs) – that are responsible for well defined infrared emission features[4,5] and contribute to the grain chemical activity. Thus, in all but the coldest regions of the ISM, H_2 is formed on a graphitic-like surface, making hydrogen–graphite systems valuable models for studying hydrogen formation in space.[6–11]

Just like any gas–surface reaction, H_2 recombination can occur through three different mechanisms: Langmuir–Hinshelwood (LH), Eley–Rideal (ER) and Hot-Atoms (HA). In the LH mechanism, both reactants are adsorbed on the substrate and diffuse until they meet each other and react. The ER mechanism occurs when only one of the reactants adsorbs onto the surface, and the second comes directly from the gas phase and forms the product molecule in a direct collision. The HA process is intermediate, since one of the reactants is trapped on the surface but not equilibrated, hence it typically diffuses hyperthermally until it encounters the reaction partner. The actual mechanism of hydrogen formation strongly depends on the physical conditions

[a] *Università degli Studi di Milano, Dipartimento di Chimica, via Golgi 19, 20133 Milano, Italy. E-mail: rocco.martinazzo@unimi.it*
[b] *Institute of Physical and Theoretical Chemistry, Goethe University Frankfurt, Max-von-Laue-Str. 7, D-60438 Frankfurt/Main, Germany*
[c] *Consiglio Nazionale delle Ricerche, Istituto di Scienze e Tecnologie Molecolari, Milano, Italy*

considered – mainly the temperature of the grains (T_s) and that of the gas phase (T_g) – since these determine whether the reactants chemisorb on the surface or bind only weakly to it.

Physisorption of hydrogen atoms on the basal (0001) surface of graphite is barrierless and, in principle, may occur easily but in practice it is rather inefficient[12] because projectile atoms hardly get rid of their excess energy to get trapped on the surface. Physisorbed H atoms quickly diffuse from one adsorption site to the other, even at extremely low temperatures, thanks to tunneling through the small ($\sim$5 meV) diffusion barriers.[13] Hence, physisorbed species can lead to H_2 formation through any of the above mechanisms, namely LH,[14] HA or ER.† [8,10] However, the physisorption well is so shallow ($\sim$40 meV)[15] that complete desorption already takes place at $T_s \sim$ 30–40 K. Hence, physisorbed hydrogen atoms are absent in those regions of the ISM where the grain temperature exceeds a few tens of Kelvin.

On the other hand, chemisorption of hydrogen atoms involves the formation of a strong covalent bond with a carbon atom of the substrate, a process that produces an extended surface puckering and requires some energy to occur. In fact, upon chemisorption, the binding C atom‡ moves out of the surface plane by about 0.4 Å as a consequence of the $sp^2 \rightarrow sp^3$ re-hybridization of its valence orbitals,[16–20] and stores a considerable amount of energy ($\sim$0.8 eV) in the form of a lattice deformation. Chemisorbed H atoms are immobile on the surface because a high barrier separates neighboring sites (in fact, the height of the diffusion barrier matches the desorption threshold[21]), thus LH between chemisorbed species is ruled out and only ER/HA reactions are left to form molecular hydrogen.

The Eley–Rideal reaction alone is considered to be a reasonably efficient route to H_2, the main limitation being the presence of some chemisorbed species. Indeed, the reaction cross-sections for this process have been found to be rather large, both theoretically[6,8] and experimentally[22] (*i.e.* much larger than that found for the same process on metal substrates[23]) and the overall efficiency of the mechanism only depends on the ability of a H atom to overcome the $\sim$0.2 eV high barrier to sticking.§ The latter seems to be rather poor in direct collisions[25] but it is worth noticing that facile sticking is possible at defective sites (vacancies, voids, amorphous islands, edges, *etc.*) where a small – if not vanishing – barrier can be found. In addition, sticking may also occur through tunneling from the physisorbed state in times that could yet be small on an astronomic time-scale, and hence physisorbed atoms on low temperature grains may have enough time to find their way to a stable chemisorption site.

The Eley–Rideal formation of H_2 on graphitic substrates is a barrierless and highly exothermic ($\sim$3.9 eV) reaction. Hence, determining the correct partitioning between the internal and translation energy of the nascent molecule, as well as the amount of energy left on the surface, is important for the energy balance of the gas and the solid phase. Furthermore, the ro-vibrational distribution of H_2 is a key issue for the chemistry of the ISM, since vibrational excitation may help in overcoming activation barriers and may make endothermic reactions possible, *e.g.* $H_2 + C^+ \rightarrow CH^+ + H$.[26,27]

To date, several specific aspects of the dynamics have been addressed[6–10,28–38] (the size of the cross-sections,[6,8,32,36,37] the internal excitation of the product molecules,[6–8,10,28–32,36,37] the role of the collision energy and of the vibrational excitation of the adsorbate,[6,8,28,32] the effect of isotopic substitutions,[38,39] *etc.*) upon resorting to various approximations, either in the dynamics or in the model. However, the (dynamical) role of the lattice, as well as its ability to absorb part of the reaction energy, has received little attention. Molecular dynamics[9] and *ab initio* molecular dynamics[36,37] investigations assessed the role of the substrate in a classical setting – with a focus on the surface corrugation and on the competing processes that reduced dynamical models neglect – though some attempts have been made to describe the surface quantally in a mixed quantum-classical approach.[29] Quantum dynamics has so far been restricted to reduced dimensional models that completely neglect the dynamical role of the substrate,[8,32,33,38] or reduce it to that of the binding carbon,[7,31] at the expense of other degrees of freedom (DOF). Thus, a complete and consistent description of the reaction dynamics is still lacking, mainly because the high dimensionality of the problem has yet prevented a fully quantum modeling of the reaction dynamics that appears essential for a correct description of the process.

In this paper, we make a step forward in this direction and, while focusing on a collinear approach, we investigate the Eley–Rideal H_2 forming reaction on graphite including for the first time the lattice in a full quantum setting. We employ a system-bath model that has been recently developed and successfully used for studying hydrogen sticking on the same substrate, in a full quantum setting.[25,40] The model describes the main reactive system – here the two H atoms and the binding carbon – subjected to (state-independent) frictional-fluctuating forces appropriate for a graphitic substrate, conveniently mapped into an (equivalent) Independent Oscillator (IO) Hamiltonian.[41–47] The advantage of such a description is that the ensuing Hamiltonian dynamics can be investigated with high-dimensional, numerically exact quantum methods. For the latter, we opted for the powerful multi-configuration time-dependent Hartree (MCTDH) method[48–50] and, in particular, for its recent Multi-Layer variant (known as ML-MCTDH) that has considerably extended the limits of applicability of a multiconfiguration approach.[51–53] Additionally, we also performed classical and quasi-classical calculations on the same model to assess the reliability of classical dynamics, eventually corrected for quantum effects, in describing the reaction dynamics.

This paper is organized as follows. Section 2 details the adopted system-bath model and the methodology used to simulate the dynamics, Section 3 describes our findings and Section 4 summarizes and concludes the work.

† Strictly speaking, because of the above mentioned high mobility of physisorbed H species, the term Eley–Rideal might be inappropriate in this context.

‡ The same happens for its neighbors, though to a lesser extent.

§ An accurate estimate of the sticking barrier has been recently obtained with vdW-inclusive DFT calculations calibrated on MP2 results, and amounts to 179 $\pm$ 5 meV.[24]

2 Theory

2.1 Dynamical models

The details of our general system-bath strategy have already been reported in our previous works,[25,40,46,47,54] so here we limit ourselves to a short description of the model, focusing on the features relevant to the specific case of the Eley–Rideal recombination.

In order to simulate the title reaction, we represent a projectile atom, the so-called 'incidon', which collides with a chemisorbed target atom, the so-called 'targon', here limiting the approach to the collinear configuration. The target H atom is bound to a substrate C atom, initially at rest in its puckered position. These three atoms form the main reactive system. The C atom is bilinearly coupled with a bath of harmonic oscillators (HOs) which replaces the rest of the lattice, and the HO frequencies and coupling coefficients are designed to describe the fluctuating–dissipative properties of a graphitic substrate. The Hamiltonian takes an Independent Oscillator (IO) form in which the bath couples only to the height z_C of the binding C atom above the surface, a rather reasonable approximation for the process at hand that was already successfully employed in investigating the sticking dynamics.[25,40] Specifically, the adopted Hamiltonian reads as

$$H = \frac{p_i^2}{2m_i} + \frac{p_t^2}{2m_t} + \frac{p_C^2}{2m_C} + V(z_i, z_t, z_C) + \sum_k \left[\frac{p_k^2}{2m} + \frac{m\omega_k^2}{2}\left(q_k - \frac{c_k z_C}{m\omega_k^2} \right)^2 \right] \quad (1)$$

where $z_i(z_t)$ represent the height of the incident (target) H atom above the surface, $p_i(p_t)$ its conjugate momentum and $m_i(m_t)$ its mass, p_C is the momentum conjugate to z_C and m_C the mass of the C atom. These dynamical variables form the 'reagent' set of coordinates, shown in blue in Fig. 1, which is appropriate to compute total reaction probabilities and energy partitioning between the molecule and the surface. A 'product' set of coordinates (in red in Fig. 1), on the other hand, suits better to the calculation of the vibrational populations of the reaction product. In this case, the dynamical variables are the H_2 center of mass height $Z = (m_i z_i + m_t z_t)/(m_i + m_t)$ and the relative distance between the two hydrogen atoms $z = z_i - z_t$.

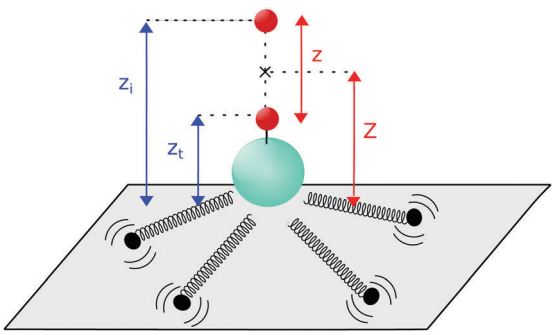

Fig. 1 The "reagents" set of coordinates in blue and the "products" set of coordinates in red.

Furthermore, in eqn (1), q_k and p_k denote the position and momentum of the k-th bath oscillator and the mass m is conveniently chosen, without loss of generality, to be the same for each oscillator. Importantly, the frequencies ω_k and coupling coefficients c_k sample the so-called spectral density of the environmental coupling that fully characterizes the generalized Langevin dynamics of the binding carbon atom. In fact, this spectral density ($J_C(\omega)$ in the following) relates to the frequency dependent memory kernel $\tilde{\gamma}_C(\omega)$ describing the frictional forces acting on C through the standard relation[41,45] $J_C(\omega) = m_C\omega\Re\tilde{\gamma}_C(\omega)$, and links to fluctuations *via* a fluctuation-dissipation relation. $J_C(\omega)$ thus contains all the information about the coupling between the carbon atom and the rest of the graphitic surface. It was first derived in ref. 40 when investigating the hydrogen sticking dynamics on the same substrate[25] and clearly applies unaltered to the present problem. We adopted here a standard sampling of $J_C(\omega)$ giving the frequencies a uniform spacing $\Delta\omega$ and setting the coupling coefficients c_k according to

$$c_k = \sqrt{\frac{2m\omega_k \Delta\omega J_C(\omega)}{\pi}} \quad (2)$$

though optimal sampling schemes can be devised.[55]

Finally, $V(z_i,z_t,z_C)$ is an analytic potential describing the interactions within the main system. We built it by modifying the well established, rigid-surface LEPS potential $V_{LEPS}(z_i,z_t)$ of Sha *et al.*[6] – here limited to the collinear configuration – to include a potential term $V_{CH}(z_t,z_C)$ describing the perpendicular motion of the C atom in the presence of the chemisorbed H atom,

$$V(z_i,z_t,z_C) = V_{LEPS}(z_i - z_C, z_t - z_C) + V_{CH}(z_t,z_C) - V_t(z_t - z_C) \quad (3)$$

Here $V_{CH}(z_t,z_C)$ is the DFT-based potential developed by Kerwin *et al.*[56] to describe the sticking of a H atom on a graphitic substrate, the coupling between the reacting hydrogens and the C atom is given in a surface-oscillator (SO)-like form (first term on the r.h.s.) and $V_t(z)$ is a counter-term avoiding double counting (it is the adsorption profile of the target H with the C atom in its puckered position). Furthermore, consistent with the SO-like form of the coupling, $V_{LEPS}(z_i,z_t)$ was set to be the type A potential of ref. 6, *i.e.* the one describing hydrogen recombination in the diabatic limit where the C atom remains frozen in its puckered configuration.

Overall, the interaction potential $V(z_i,z_t,z_C)$ preserves the main features of the LEPS potential, showing a downhill, barrierless path to the reaction product, if not for a (spurious) tiny barrier in the entrance channel ($\sim$10 meV high) that does not affect the dynamics at the collision energies E_{coll} considered in this work ($E_{coll} \geq 0.2$ eV), and that should be removed when considering lower collision energies. In fact, it is now widely accepted that Eley–Rideal formation of H_2 on graphite is truly barrierless.[35] Apart from this artifact, the adopted potential energy surface (PES) provides a reasonably good representation of the system energetics. The H atom adsorption energy is -0.66 eV and the equilibrium heights of the C and H atoms above the surface plane are 0.37 Å and 1.48 Å, respectively.

Hence, with a H_2 binding energy of 4.58 eV the reaction exoergicity is $\sim$3.9 eV when uncorrected for the zero-point-energies (ZPEs).

Finally, starting from the high dimensional model of eqn (1) we devised simpler, lower dimensional models – one 3D and one 2D – to investigate the role that the substrate plays in the dynamics. In the 3D model we removed the bath, while keeping the C atom dynamically active, to assess whether dissipation affects the reaction dynamics. This approximation captures recoil effects, and provides reasonable averaging of the reaction outcome over the initial state of the substrate. The 2D model, on the other hand, further neglects the C atom dynamics and uses the potential $V(z_i,z_t,z_C^{eq})$ (where z_C^{eq} is the equilibrium height of the C atom in the hydrogeneted surface) to describe the interactions between the two atoms and between the atoms and the surface. It corresponds to the diabatic approximation where the C atom is frozen in its puckered position during the entire dynamics. The model thus neglects any dynamical effect of the substrate, though accounts by construction for the static ones.

2.2 Wavepacket dynamics

We performed several quantum dynamical calculations with the multi-layer multi-configuration time-dependent Hartree[48–50] method, which is particularly efficient when propagating many DOFs. In this method the wavefunction is expanded as a combination of Hartree products of time-dependent single-particle functions of combined modes (*i.e.* groups of the original variables), like in the original MCTDH method, but the latter are further expanded in a MCTDH fashion, using smaller dimensional modes. The procedure can be arbitrarily repeated to generate a 'tree' until reaching the lower level of description, which is in terms of a primitive (time-independent) grid for each coordinate. Expansion coefficients and single-particle functions are then evolved in time following variational equations of motion, and the wavefunction can be analyzed for the quantities of interest.

We performed our calculations using the powerful MCTDH Heidelberg package,[57] which is the first implementing the ML-MCTDH method for arbitrary trees.[53] Fig. 2 and 3 give a representation of the ML-MCTDH wavefunctions employed in our simulations. We used a bath of 32 harmonic oscillators, uniformly spaced in frequency in the range 0–900 cm^{-1}, since this number is large enough to guarantee a Poincaré recurrence time t_P much longer than the reaction dynamics ($t_P \sim 1200$ fs) and turn it effectively dissipative. As a consequence of the uniform sampling, the coupling coefficients c_k, were set according to eqn (2), using the spectral density $J_C(\omega)$ derived in ref. 40. As for the single-particle functions of our wavefunctions we chose to group the degrees of freedom of the reactive system in a single 3D combined mode, while the bath DOFs were arranged in 2D modes within multi-layer expansions, which were designed differently for the 'reagent' (Fig. 2) and for the 'product' (Fig. 3) set of coordinates. We found the results rather insensitive to the adopted ML tree (likely because the reaction dynamics is much faster than bath relaxation, see below) though the second scheme, Fig. 3, where the system couples directly to near-resonant oscillators, turns out to be computationally more efficient. As for the primitive grids, we used a Hermite basis for the harmonic oscillator DOFs $\{q_k\}$ (see bottom of Fig. 2 and 3), and uniform grids for the system degrees of freedom (Table 1).

The initial wavefunctions were of the product form, a wavefunction for the projectile times a wavefunction for the rest, and represented a hydrogen atom scattering off a target hydrogen atom equilibrated with a T_s = 0 K surface. The projectile wavefunction was chosen to be a Gaussian wavepacket with an average initial momentum directed towards the surface and sufficiently narrow in momentum space to be representative of the corresponding average energy. The 'target' wavefunction, on the other hand, was the ground-state wavefunction describing a H atom bound to the C atom that in turn coupled to the bath. The whole initial wavefunction was obtained from a relaxation run

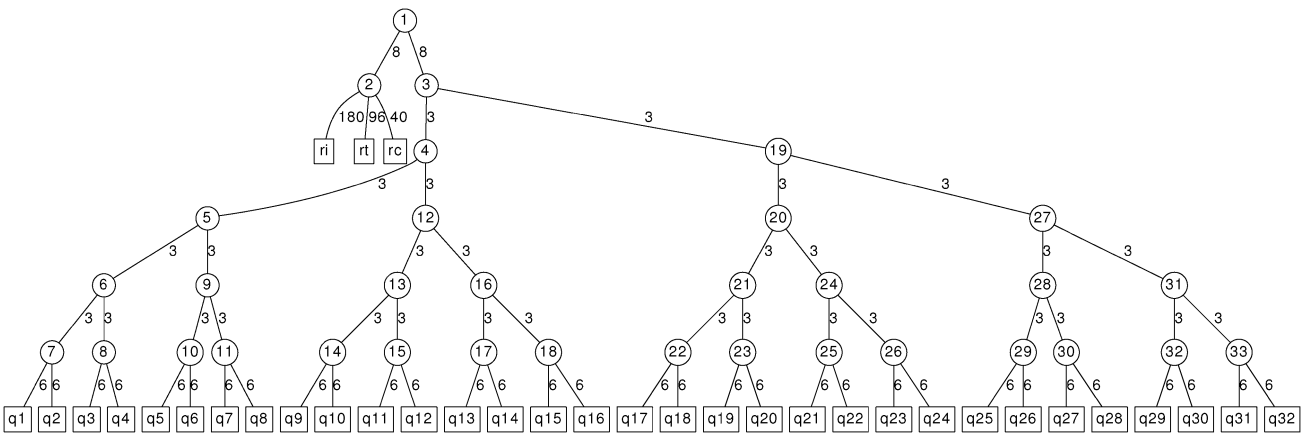

Fig. 2 Multi-layer tree used in the reagent set of coordinates (here ri, rt and rc stand for z_i, z_t and z_C, respectively). Each circle denotes a MCTDH-like wavefunction in the tree, along with its modes (the arms) and the number of the single particle functions used in the expansion (the numbers on the arms). The squares at the bottom layers are for the primitive modes and the numbers in this case represent the size of the primitive grids.

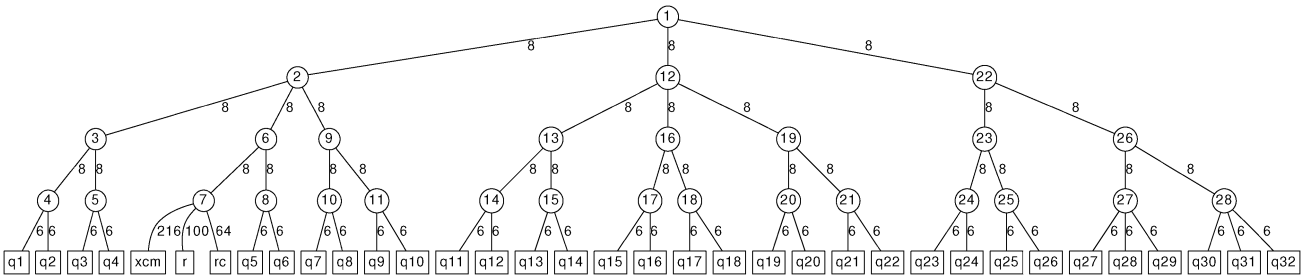

Fig. 3 The same as in Fig. 2 but for the product set of coordinates (here xcm, r and rc stand for Z_{cm}, z and z_C, respectively).

Table 1 Left (min) and right (max) bounds of the grids (in atomic units) and number of points (n_X) used in the 2D, 3D and high dimensional calculations, for both the 'reagent' (z_i and z_t) and the 'product' (Z and z) set of coordinates of the main system

	2D	3D	Full
z_i^{min}	2.5	2.5	2.5
z_i^{max}	18	16	21
n_i	144	144	180
z_t^{min}	1.0	1.0	1.0
z_t^{max}	12.0	12.0	12.0
n_t	108	108	96
Z^{min}	2.0	2.0	2.0
Z^{max}	20	20	20
n_Z	225	225	216
z^{min}	0	0	0
z^{max}	20	20	20
n_z	144	256	100
z_C^{min}	—	−1.5	−1.5
z_C^{max}	—	2.2	2.2
n_C	—	64	40

(*i.e.* propagation in imaginary-time) that used a modified Hamiltonian, namely

$$\begin{aligned} H^{\text{relax}} &= \frac{(p_i - p_0)^2}{2m_i} + \frac{\hbar^2}{2m_i \Delta z^2}(z_i - z_0)^2 \\ &+ \frac{{p_t}^2}{2m_t} + \frac{{p_C}^2}{2m_C} + V_\infty(z_t, z_C) \\ &+ \sum_k \left[\frac{{p_k}^2}{2m} + \frac{m\omega_k^2}{2}\left(q_k - \frac{c_k z_C}{m\omega_k^2} \right)^2 \right] \end{aligned} \tag{4}$$

where p_0 is the average momentum of the projectile, Δz is the spatial width of the Gaussian wavepacket and $V_\infty(z_t,z_C)$ is the asymptotic interaction potential, $V_\infty(z_t, z_C) = \lim_{z_i \to \infty} V(z_i, z_t, z_C)$.

This form of the Hamiltonian ensures that the desired initial state is the long time limit of the imaginary-time dynamics, irrespective of the coordinates used to represent the wavefunction. Once the correct initial state was obtained, real time propagation was performed using the Hamiltonian of eqn (1), adding only cubic absorption potentials at the edges of the (z_i,z_t) grid to avoid artificial reflections of the wavepacket and allow analysis of the results. Time-energy mapping of the flux was not feasible for our high-dimensional wavepacket calculations and, as mentioned above, we resorted to sufficiently narrow wavepackets that were representative of the average energy of interest. We checked, though, in the 2D and 3D simulations that such a procedure gives results in excellent agreement with the energy-resolved total reaction probabilities obtained from the time-energy mapped flux along z_t in the 'reagent' set of coordinates.

Total reaction probabilities were computed in the 'reagent' set of coordinates using the average flux absorbed along z_t. Calculations in the 'product' set, on the other hand, were used to extract the vibrational populations of the product molecular hydrogen, as well as the average internal and kinetic energy of the molecule and the energy transfer to the substrate. In particular, since the latter are referenced to the reacted fraction of the wavepacket only, we employed standard product projection operators h—*i.e.*, $h(\mathbf{x}) = 1$ for $\mathbf{x}$ in the product channel and $h(\mathbf{x}) = 0$ otherwise—to evaluate expectation values normalized to a reactive event,

$$E_R[\Psi] = \frac{\langle \Psi | h \hat{R} h | \Psi \rangle}{\langle \Psi | h | \Psi \rangle}$$

Here R is the observable of interest, *e.g.* the internal and kinetic Hamiltonians of the H_2 molecule, the projector onto a vibrational state of H_2, *etc.*

We also performed classical and quasi-classical trajectories in the microcanonical ensemble, using the system-bath Hamiltonian in eqn (1) in the 'reagent' set of coordinates. In these classical calculations the bath was made of 500 harmonic oscillators, which were arranged uniformly in the same range as above (0–900 cm^{-1}) with coupling coefficients sampling the spectral density $J_C(\omega)$. This gave rise to a recurrence time much larger than in the quantum simulations ($t_P \sim 18$ ps) that allowed us to perform unrestricted checks of convergence with respect to propagation times. The initial states of the trajectories were chosen differently according to the recipes for either a classical or a quasi-classical dynamics. In the first case, the bath was prepared with an equilibration run at a given surface temperature (1 K, 5 K, 100 K and 300 K), using Langevin dynamics to obtain the desired temperature. In the quasi-classical simulations at 0 K, on the other hand, the zero point energy of the substrate was taken into account, and the initial state of the trajectories was chosen by sampling the quantum ground state of the surface. Specifically, the equilibration step was replaced by a random pick of coordinates and

momenta from the phase-space orbits of the normal modes of the surface (*i.e.* the target hydrogen atom, the binding carbon and the harmonic bath) at the energy of their (quantum) ground-state. For both classical and quasi-classical trajectories, in order to evaluate the H_2 energy components and the amount of energy transfer to the substrate, we computed the average energies considering the reactive trajectories only.

3 Results

In the following, we present the results of the quantum, the quasi-classical and the classical calculations that we performed in order to investigate the Eley–Rideal H_2 recombination on graphite. The results from the three different substrate approximations are also shown.

Fig. 4 gives an overview of the results of a typical quantum dynamical simulation: here the one-dimensional densities along z_C (left panel) and z_t (right panel) are reported at different times—from bottom to top, well before the collision, at the collision instant and after the collision—for a projectile energy of ~1.1 eV. As it can be seen for that figure, the wavepacket, initially localized to describe the CH moiety above the surface, broadens and distorts during the collision and splits afterward to describe a reacted (small z_C and large z_t) and a reflected (larger z_C and small z_t) fraction. This is best seen in Fig. 5, where the same one-dimensional densities are plotted over time, though now the wavepacket is absorbed at the grid edges and disappears from the grid. For the chosen initial state the collision occurs after about 35–40 fs of propagation, and appears to be a rather direct process, with no evident signature

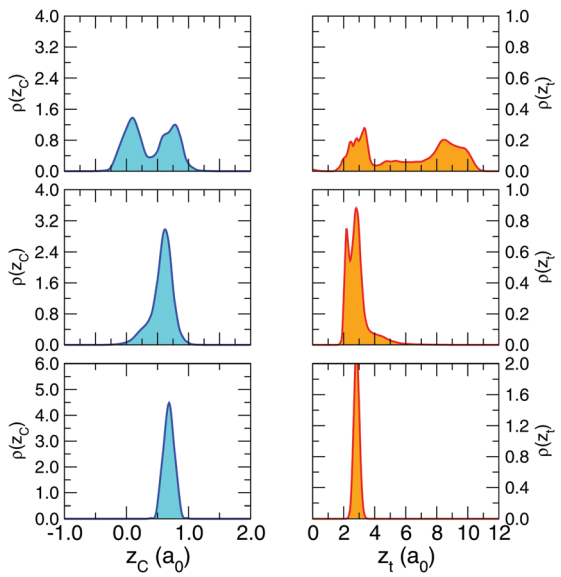

Fig. 4 Time evolution of the reduced densities along z_C (left panel) and z_t (right panel) obtained from the quantum simulations using the high dimensional dynamical model at different times, t = 0, 30 and 60 fs from bottom to top. The latter correspond respectively to a time before, during and after the bouncing of the projectile off the target. The data refer to a collision energy of ~1.1 eV.

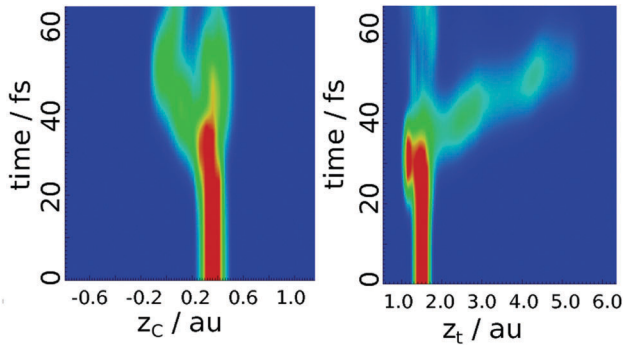

Fig. 5 Time evolution of the reduced densities along z_C (left panel) and z_t (right panel) from the same calculations of Fig. 4.

of multiple rebounds. The target atom presses the binding C atom on the surface, and the latter recoils and eventually pushes the H atom towards the projectile. In this reactive fraction z_t moves away from the surface and the binding carbon, now performing large amplitude oscillations around the equilibrium position of the flat surface, starts relaxing and decays towards its final equilibrium position z_C = 0. This relaxation process starts soon after the product molecule left the surface, and is signaled by the shrinking of the left branch of the wavepacket pictured in Fig. 5, left panel. At the same time, energy is transferred to the rest of the lattice, and is distributed to the bath oscillators in a way which is determined

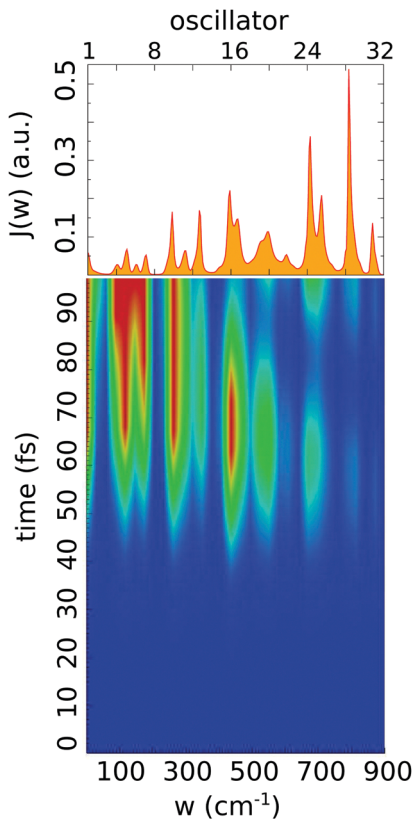

Fig. 6 Average excitation number of the bath oscillators. The data refer to the same collision energy of Fig. 4.

by the coupling. This can be seen in Fig. 6, which reports the average number of phonons in the bath during the dynamics, along with the spectral density $J_C(\omega)$ governing the system-bath coupling. Relaxation of the C atom—*i.e.* the unpuckering of the surface—is rather fast, and is completed in tens of fs, in accordance with the similar behavior found for the surface mode describing block oscillations of the CH moiety in the H-graphene system.[40] This is due to the fact that the frequency of the carbon atom vibrator normal to the surface (834 cm^{-1}) is well within the spectral range of the bath.

As for the reflected fraction of the wavepacket, on the other hand, it describes a situation where both z_C and z_t remain close to their initial equilibrium value, only slightly vibrationally excited as is evidenced by the broadening of the wavepacket. Here, relaxation involves the carbon–hydrogen stretching; it is fast (few ps)[40,58] but occurs on a much longer time-scale than the one relevant for the reaction dynamics.

3.1 Reaction probabilities

Fig. 7 shows the reaction probabilities P_{ER} as a function of the collision energy, as obtained from the quantum, the quasi-classical and the classical calculations using the high-dimensional model of eqn (1). Classical simulations were performed at two different surface temperatures, a high value (300 K) and a low value (1 K) mimicking scattering off a surface in its classical ground state.

The probability curves share a similar trend, featuring a minimum at intermediate values of the collision energy, whose exact position depends on the type of calculation. This minimum results from the smoothening of the low-T_s classical results, which show no reaction in a sharply defined energy range, $\sim$0.2–0.7 eV. The decrease of P_{ER} for decreasing energy is common to many other calculations[10,35] but its increase at low energies is a peculiar feature risen by the adopted potential, at odds with previous works.[8,10,11] This effect is also present in the results of the reduced-dimensional 2D calculations (see below) that made use of the same LEPS potential of previous works,[6] except for the refinements of the CH interaction detailed in eqn (3), *i.e.* the replacement of the Morse-like adsorption profile of the targon—implicit in the LEPS potential—with a more accurate term describing also the C atom dynamics.¶ Hence, it is most likely due to some minor change in the PES at short range and it shows up here because, in the absence of a barrier, the shape of the PES determines the (collinear) reaction probabilities to a large extent.[35] It was indeed shown that tiny changes in the PES in the interaction region—such as those related to the theory level employed for the electronics or to the adopted surface model (*i.e.* cluster *vs.* periodic slab)—modify the shape of the elbow and change the energy dependence of the reaction probability.[35]

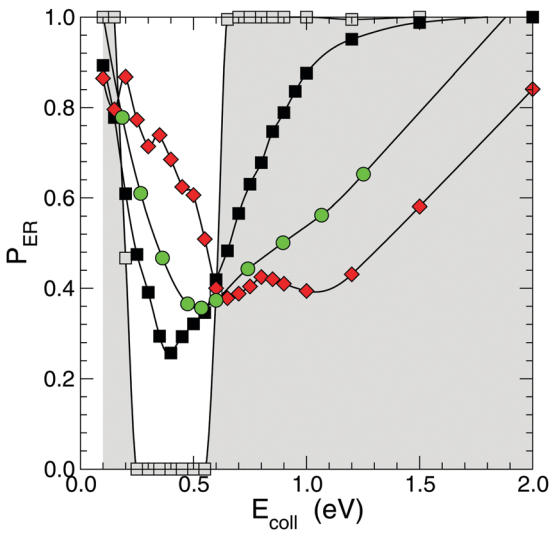

Fig. 7 Eley–Rideal reaction probabilities as a function of the collision energy E_{coll}, as obtained with classical (squares), quasi-classical (diamonds) and quantum (circles) calculations using the high dimensional Hamiltonian of eqn (1). Classical results refer to two different surface temperatures, namely grey symbols (and shaded area) for T_s = 1 K and black symbols for T_s = 300 K.

From Fig. 7 it is evident that the classical results are only qualitatively similar to the quantum ones, though the latter always fall in between the limits provided by the (high temperature) classical simulations and the quasi-classical results. Hence, even though the agreement is not as good as for the sticking case,[25] classical mechanics does a reasonably good job in describing the reaction, provided the lattice and the binding C atom are given some energy that can mimic the quantum fluctuations of the substrate. In fact, as mentioned above, the classical data at the lowest temperature considered (1 K) show a different behavior, with sharp transitions between 100% reaction and no reaction at all, suggesting that the initial condition of the substrate plays a primary role in determining the outcome of the collision.

Further insights into the reaction dynamics are obtained by comparing different dynamical models in the quantum setting. Fig. 8 shows the results obtained from two reduced-dimensional quantum calculations (the 2D and the 3D model described in Section 2.1) along with those of the high dimensional model, eqn (1). This figure unambiguously shows that the main effect of a movable substrate comes from the carbon atom dynamics. The results of the rigid substrate case (2D case, black line in the plot), though having a similar trend, compare only qualitatively with the results of the calculations in which C was allowed to move. In particular, the carbon dynamics shifts—roughly rigidly—the reaction probability curve to higher energies and thus leads to an increase of P_{ER} at low energies, while for $E_{coll} \gtrsim 0.5$ eV the trend is reversed.

Importantly, there is almost no difference between the results from the 3D and the full calculations (respectively, red line and green circles in Fig. 8), thereby suggesting that the reaction dynamics is so fast, compared to the C atom dynamics, that the fate of the C atom after the impact of the two hydrogens—*i.e.* whether it quickly relaxes or vibrates indefinitely—has little effect on the outcome of the collision. This result partly justifies the numerous studies which kept the substrate frozen: the lattice atoms play only a passive role in the dynamics, with

¶ It is not guaranteed though that when freezing the C atom the ensuing 2D potential is more accurate than the original one.

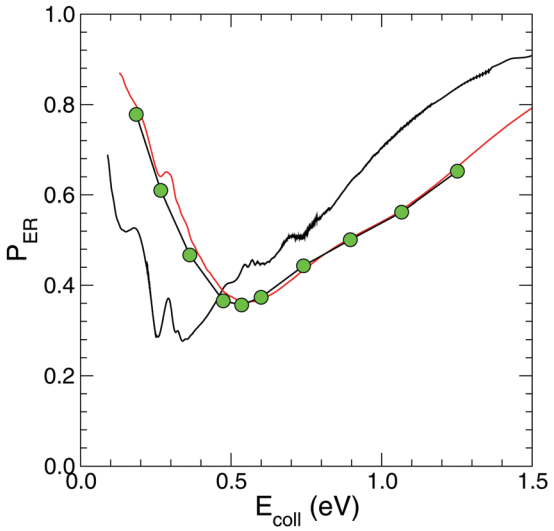

Fig. 8 Quantum reaction probabilities as a function of the collision energy, as obtained from reduced-dimensional calculations (black and red lines for 2D and 3D models, respectively) and from the high dimensional calculations using the Hamiltonian of eqn (1) (see the text for details).

the important exception of the binding C atom which does affect the reactive event and needs to be explicitly described to obtain a correct description of the reaction.

It is worth noticing in this context that attempting to reduce the effect of the C atom to a static one—*i.e.* by averaging 2D diabatic results over the appropriate distribution of the initial position of the C atom, according to what is known as 'phonon sudden approximation'[47,59]—is only partially successful. In fact, because of the SO-like coupling employed in our modeling (eqn (3)), here the sudden approximation to the dynamics would precisely reduce to a single frozen-surface calculation with the potential $V(z_i,z_t,z_C^{eq})$, and Fig. 8 shows that this is only qualitatively similar to the exact result. Even worse, an adiabatic approximation where the 2D PES implicitly describes a C atom that instantaneously relaxes during the dynamics, is not even in qualitative agreement with the results of Fig. 8 (not shown). This is mainly due to the strong interaction between the two hydrogen atoms which makes the reaction dynamics fast irrespective of the initial energy of the projectile, and thus the failure of the adiabatic approximation likely extends to the vanishingly small collision energies which are more relevant for the ISM.

3.2 Energy transfer

Next, we consider the amount of energy transferred to the surface. We are interested in the energy released for each reactive event, since this gives valuable information on the reaction dynamics.

The appropriate definition of energy transfer is a bit subtle, since the substrate prior to collision (the hydrogenated surface) differs from the substrate after a (reactive) collision has occurred (the bare surface). In addition, if we want to compare unambiguously the quantum and classical results, we must be careful in handling zero-point energies, where present. To this end, we define the internal energy of the substrates as $E_X^{int} = E_X - E_X^0$, where X = CH, C labels the hydrogenated and the bare surface, respectively, and 0 stands for the corresponding ground-state, being it quantum or classical depending on the setting. Then, the energy transferred to the surface reads simply as

$$\Delta E_s = E_C^{int} - E_{CH}^{int} \quad (5)$$

In fact, the overall energy partitioning can be described as follows. The pre-collisional energy is given by $E_i = E_{coll} + E_{CH}^{int} + E_{CH}^0$, where E_{CH}^{int} is the internal energy appropriate to the equilibrated hydrogenated surface ($\equiv$0 in the case considered in this work), whereas the post-collisional one reads as $E_f = \varepsilon_K + \varepsilon_{int} + E_{mol}^0 + E_C^{int} + E_C^0$, where ε_K and ε_{int} are the kinetic and internal energy of the product molecule, respectively, and E_{mol}^0 the ground-state energy of H_2. Since

$$\Delta E_{reac}^0 = E_C^0 + E_{mol}^0 - E_{CH}^0 \quad (6)$$

is (minus) the reaction exothermicity, the energy at disposal of the products reads as

$$E_{avail} = -\Delta E_{reac}^0 + E_{coll} \quad (7)$$

and appears correctly partitioned between the surface and the molecular components

$$E_{avail} = \Delta E_s + \varepsilon_K + \varepsilon_{int} \quad (8)$$

In practice, application of eqn (5) requires determination of the ground-state energy of the substrate for both X = C and X = CH. In the quantum case this is accomplished with imaginary-time propagations using the substrate-only Hamiltonian, whereas for the classical case this just requires a structural optimization of both the hydrogenated and the bare surface. Normal mode analysis of the equilibrium configuration further provides the necessary vibrational frequencies for defining the zero-point energy appropriate for the quasi-classical calculations (for X = CH this is in any case necessary to set the initial state of the substrate).

The results of such calculations in the energy range considered above are reported in Fig. 9 for both the quantum, the classical (at 300 K) and the quasi-classical simulations. All the curves have a similar trend, slightly decreasing and then increasing for increasing collision energy, and the energy transferred to the substrate is approximately between 0.5 eV and 1.0 eV. In particular, the most reliable quantum results depend only weakly on the collision energy and give a value of ΔE_s very close to the energy stored in the surface puckering ($\sim$0.8 eV, the dashed horizontal line in Fig. 9). This is consistent with the previous findings: the reaction dynamics is fast compared to the C atom dynamics and most of the energy stored as lattice deformation remains in the substrate. Hence, even though the dynamics of the C atom is essential for the correct description of the reaction (see Section 3.1), the binding substrate atom exchanges little energy with the reacting partners. In fact, this 'energy exchange' is essentially from the substrate to the H atoms and is $\sim$0.1 eV at most for $E_{coll} \sim$ 0.7–0.8 eV, *i.e.*,

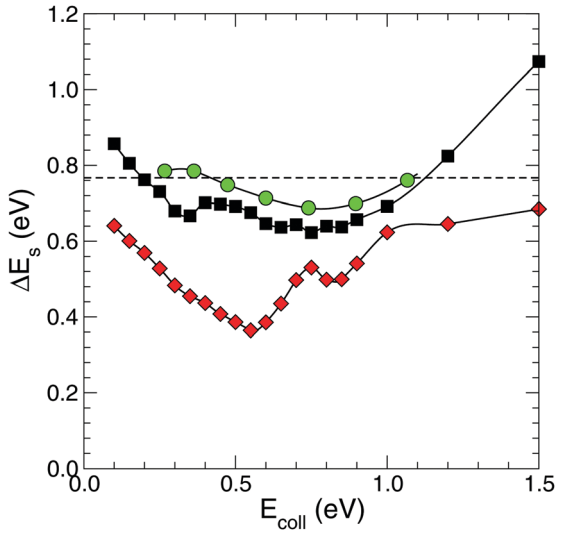

Fig. 9 Energy transferred to the substrate per reaction event, as obtained from classical (T_s = 300 K, squares), quasi-classical (diamonds) and quantum (circles) calculations at different collision energies. The horizontal line is the reference 'puckering energy' which is stored in the CH bond before the reaction has occurred.

when ΔE_s lies clearly below the nominal value of the puckering energy.

Surprisingly, Fig. 9 also shows that purely classical mechanics performs better than QCT in reproducing the energy transfer, and CT results closely follow the quantum ones in the energy range 0.2–1.0 eV. This is most likely due to the approximate way in which zero-point energies are handled in QCT.

Overall, our findings show that the energy transferred to the lattice is significant, and that formation of hydrogen molecules considerably heats the interstellar grains. To give an idea, as already observed previously,[37] we can estimate from this value the temperature increase per reaction event of a typical carbonaceous interstellar grain. This follows from the low temperature Debye expression of the specific heat, $c_v = 12\pi 4/5nk_B(T/\Theta)^3$, where $n \sim 4/35.3 \times 10^{30}$ m^{-3} is the number density of carbon atoms in graphite and $\Theta_D \sim 400$ K is its Debye temperature. For a typical grain 1 μm^3 sized at $T = 5$ K we find that formation of a single H_2 molecule increases the temperature of the grain by 2.2×10^{-4} K, a rather large value for a single molecular event. Overall, one should further consider the energy dissipated in chemisorbing the first H atom (~0.7 eV with our potential), so the total temperature increase for each H_2 molecule that is formed from gas-phase atoms is about twice the above estimate. This finding is in sharp contrast with the situation in which two (physisorbed) H atoms recombine *via* Langmuir–Hinshelwood kinetics: in the latter case only (twice) the H atom physisorption energy would be left on the surface, with hardly any consequence for the grain temperature.

3.3 Product energies

Finally, we analyze the energy in the product molecules, investigating the effects of the substrate on the total H_2 energy and on its partitioning between vibrational and translational excitation. We evaluated the average total (ε_{tot}), vibrational (ε_V) and translational (ε_K) H_2 energies considering both the high dynamical model and the two reduced-dimensional ones described above.

Fig. 10 shows the results of our analysis in the range of the collision energies considered above. It is seen that the total energy of the newly formed molecule (top panel) increases linearly with E_{coll}, as expected from the behavior of the energy transferred to the substrate that was discussed in Section 3.2. The total energy of the product molecules is much closer to the diabatic limit (dashed black line) than to the adiabatic one (dashed blue line), though the correct description of the C atom dynamics introduces a small, energy-independent contribution from the surface (see also Section 3.2).

The collisional energy dependence of the product energy comes mainly from the kinetic rather than the internal component. As is evident from the middle panel of Fig. 10 the vibrational energy shows little variations in the range E_{coll} = 0.2–1.0 eV and takes a rather large value (~1.5 eV), even though smaller than previously obtained.[6–8,10,28–32,36,37] Importantly, comparison between the 2D and the higher dimensional models shows that the energy contribution of the lattice is sizable and goes mainly in vibrations. Correspondingly, the translational energy of the H_2 molecules is very similar in the three models, *i.e.* it is less affected by the C atom dynamics, and takes rather large values: the ratio between the translational and the vibrational energy increases from 1.3 at low energies to 1.8 at high energies. In detail, one can see from Fig. 10 that the effect of the C atom motion – a sort of 'kick' of the recoiling C atom – favors the channeling of energy into vibrations (ε_V computed with the 3D or the full dimensional model is larger by ~0.5 eV than that obtained with the 2D model) while

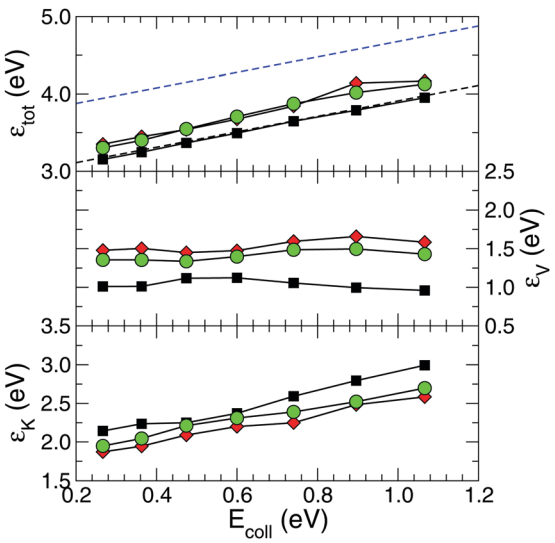

Fig. 10 Average total (top panel), vibrational (middle panel) and translational (bottom panel) energies of the product H_2 as a function of the collision energy obtained from quantum calculations. The data were obtained with three different substrate models: high dimensional (circles), 3D (diamonds) and 2D (squares). In the top panels, the solid lines represent the adiabatic (blue line) and the sudden (black line) limit for the energy transferred to H_2.

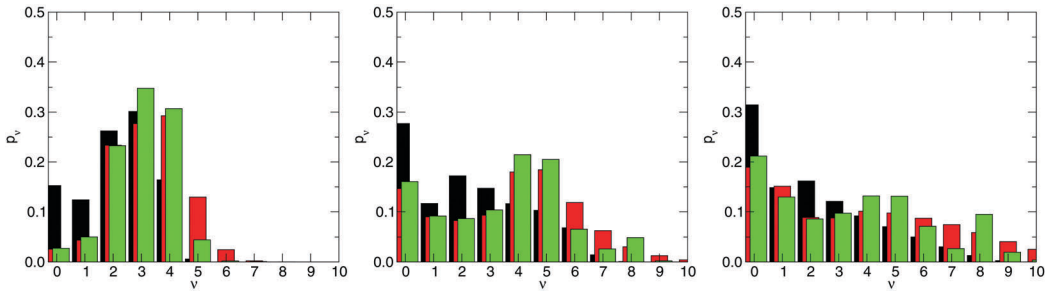

Fig. 11 Vibrational distributions from our 2D (black) and 3D (red) reduced-dimensional models along with the results obtained with the high dimensional Hamiltonian (green), for E_{coll} = 0.27, 0.74 and 1.07 eV (left, middle and right panel, respectively).

reducing the one left in translations, an effect that is slightly less pronounced when the carbon atom binds to a movable rather than a static surface.

We also obtained the vibrational populations p_v of the product molecule H_2. They are reported in Fig. 11 for selected values of the collision energy for the 2D (black bars), 3D (red) and high-dimensional (green) quantum calculations. Our potential model gives rise to vibrational distributions peaked around much lower ν than previously reported[38] (in line with the reduced internal excitation mentioned above), particularly at low collision energies. In this E_{coll} regime, other collinear models predict the maximum of the distribution to be around ν = 6, 8, while our results show that the most populated states are ν = 3, 4, incidentally closer to the experimental data by Latimer *et al.*[60] This is not due to the C atom motion; rather it appears to be mainly an effect of the adopted potential (eqn (3)) which, introducing an additional term to describe the carbon atom dynamics, necessarily modifies the entrance channel potential. In fact, the results of the 2D model, where the C atom is fixed during the dynamics, show even colder vibrational distributions than the 3D and the full dimensional model. Hence, it remains to be established whether a new fully-fledge potential energy surface including the two H atoms and the binding C atom predicts similar findings or these are artifacts of the SO-like coupling in eqn (3).

When increasing the collision energy the vibrational distributions broaden, becoming eventually bimodal with a first peak centered in the ground vibrational state of H_2 and a second peak at larger values of the vibrational quantum number, ν = 4–5. This behavior largely arises from the carbon atom dynamics, as the comparison between the 2D and the higher dimensional results reported in Fig. 11 shows.

Thus, the dynamics of the C atom not only affects the overall energy partitioning of the reaction but it also changes the shape of the vibrational distributions of H_2. The effect of the rest of the surface, on the other hand, is negligible, and this confirms the idea that the lattice dynamics gets into play right after the newly formed molecule has left the surface.

4 Summary and concluding remarks

We have investigated the collinear Eley–Rideal H_2 recombination on a movable graphitic surface by means of high dimensional wavepacket simulations with the powerful ML-MCTDH method, as well as of classical and quasi-classical trajectories calculations. The key for the application of a fully quantum approach to the reaction dynamics—one that includes the surface as an active rather than a passive player—is our system-bath modeling of the Hamiltonian. The resulting model explicitly describes the motion of the binding C atom and, using accurate information on its relaxation dynamics (as subsumed in the spectral density $J_C(\omega)$), replaces the complicated, 'atomistic' surface with a bunch of harmonic oscillators. This makes possible the use of high-dimensional wavepacket techniques to investigate a Hamiltonian dynamics that is effectively dissipative.

Our results show that the reaction probability is mainly influenced by the dynamics of the binding carbon atom. Although H_2 recombination is fast, recoil of this substrate atom does play a role in the dynamics and determines to some extent the energy partitioning. The rest of the surface, on the other hand, has a marginal effect only on the reaction. It does open efficient relaxation channels for the surface unpuckering, but only after that the molecule has left the surface. Moreover, classical and quasi-classical reaction probabilities have been shown to be in qualitative agreement only with the results of quantum simulations, thereby showing the inadequacy, especially at low surface temperature, of the classical dynamics to describe this inherently quantum system. This is mainly due to zero-point-energy effects in the dynamics, *e.g.* quantum fluctuations of the lattice, but it is not easily amended with a quasi-classical approach.

We then examined how the energy disposal is shared between the substrate and the different excitation channels of the newly formed molecule. The results show that the amount of energy left on the substrate is about the deformation energy stored in the lattice during the chemisorption of the target hydrogen atom ($\sim$0.8 eV). ΔE_s depends only weakly on the collision energy and is converted into thermal energy that considerably heats the interstellar grains. Given the low temperature of the interstellar dust grains in the diffuse clouds (T_s = 5–10 K), the estimated temperature increase of $\sim$0.4 mK for every single H_2 molecule formed *via* Eley–Rideal recombination is quite remarkable. On the other hand, E_{coll} is almost completely transferred to the product molecule. The total energy of H_2 increases linearly with the incidence energy and it is much closer to the diabatic limit than to the adiabatic one,

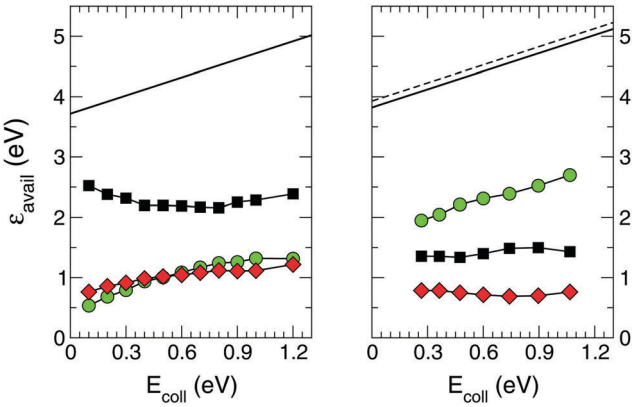

Fig. 12 Energy partitioning obtained with classical AIMD (left panel) and quantum (right) calculations. Average product energies as a function of the collision energy: internal (square symbols) and translational (circles) energy of H_2 and internal energy of the surface (diamonds). Thick lines mark the reaction exoergicity (on the right panel, thin and dashed line for ZPE and non-ZPE corrected).

thereby confirming that the carbon remains close to its puckered position and relaxes only once H_2 is formed. Explicit consideration of the C atom motion, however, promotes vibrational excitation of the product, a kind of recoil effect of the substrate atom, at the expense of the translation energy of H_2.

As a whole, our findings show the importance of including the C atom motion in the description of the reaction (and of accounting for elementary quantum effects such as the initial quantum state of the substrate). They also show, though, that the rest of the lattice plays a marginal role, at least in the collinear configuration considered here.

It remains to be established whether these findings translate unaltered to higher dimensional models where non-collinear collisions are possible and the C atom dynamics is more directly probed by the projectile atom. These non-collinear collisions are actually those determining the size of the reaction cross-section, and could play an important role in determining the energy partitioning in a more realistic situation. To show their possible effect we can tentatively compare the results of our collinear calculations with those of full dimensional (though classical) AIMD simulations[36,37] on a T_s = 0 K surface (see Fig. 12). It is evident from Fig. 12 that the energy partitioning obtained in the two cases is rather different and only the energy transferred to the lattice is in (rough) agreement between the two. It is thus important to establish whether this is an effect of the dimensionality (full *vs.* collinear), of the dynamics (classical *vs.* quantum), of the underlying potential (*ab initio vs.* 'semiempirical') or a combination thereof.

Overall, the present study represents a first attempt to describe fully quantum mechanically the coupling to phonons (and the ensuing energy dissipation) in a surface chemical reaction. The investigated system represents a rather challenging problem where a surface atom interacts strongly with the adsorbate, a condition which precludes any perturbation-theory treatment of the dynamics or coupled-channel expansion of the wavefunction. We have shown that by carefully choosing the system-bath partitioning—hence including the binding surface atom in the main system—one can describe the strong adsorbate–surface interaction with a fully correlated model, thereby broadening the range of applicability of the original independent oscillator model. The strategy appears to be rather general and, thanks to the progress in propagating high-dimensional wavepackets, can be applied nowadays to situations where several DOFs comprise the main system. Eventually, collective modes[55,61] (*e.g.* localized surface modes) may be introduced to keep the dimensionality of the main system at a tractable level.

The present work used a collinear approach to begin with but work is already in progress to extend our simulations to a 4D plus bath model that can describe non-collinear collisions. With the same token, a new subsystem potential energy surface is currently under study to overcome the limitations of the SO-like coupling appearing in eqn (3). Thus, first-principles based, unrestricted quantum dynamical studies of the title reaction might be possible in the near future with simple refinements to the approach used in the present work.

Conflicts of interest

There are no conflicts to declare.

Acknowledgements

The authors acknowledge the CINECA award under the ISCRA initiative, for the availability of high performance computing resources and support. M. B. gratefully acknowledges fellowship support by the Alexander von Humboldt Foundation.

References

1 V. Wakelam, I. Smith, E. Herbst, J. Troe, W. Geppert, H. Linnartz, K. Öberg, E. Roueff, M. Agúndez and P. Pernot, *et al.*, *Space Sci. Rev.*, 2010, **156**, 13–72.
2 D. Hollenbach and E. Salpeter, *J. Chem. Phys.*, 1970, **53**, 79–86.
3 D. Hollenbach and E. Salpeter, *Astrophys. J.*, 1971, **163**, 155.
4 B. T. Draine, *Annu. Rev. Astron. Astrophys.*, 2003, **41**, 241–289.
5 E. Herbst, *Chem. Soc. Rev.*, 2001, **30**, 168–176.
6 X. Sha, B. Jackson and D. Lemoine, *J. Chem. Phys.*, 2002, **116**, 7158–7169.
7 S. Morisset, F. Aguillon, M. Sizun and V. Sidis, *J. Phys. Chem. A*, 2004, **108**, 8571–8579.
8 R. Martinazzo and G. F. Tantardini, *J. Chem. Phys.*, 2006, **124**, 124702.
9 D. Bachellerie, M. Sizun, F. Aguillon, D. Teillet-Billy, N. Rougeau and V. Sidis, *Phys. Chem. Chem. Phys.*, 2009, **11**, 2715–2729.
10 S. Casolo, R. Martinazzo, M. Bonfanti and G. F. Tantardini, *J. Phys. Chem. A*, 2009, **113**, 14545–14553.
11 A. J. Meijer, A. J. Farebrother, D. C. Clary and A. J. Fisher, *J. Phys. Chem. A*, 2001, **105**, 2173–2182.
12 B. Lepetit and B. Jackson, *Phys. Rev. Lett.*, 2011, **107**, 236102.

13 M. Bonfanti, R. Martinazzo, G. F. Tantardini and A. Ponti, *J. Phys. Chem. C*, 2007, **111**, 5825–5829.
14 S. Morisset, F. Aguillon, M. Sizun and V. Sidis, *J. Chem. Phys.*, 2005, **122**, 194702.
15 E. Ghio, L. Mattera, C. Salvo, F. Tommasini and U. Valbusa, *J. Chem. Phys.*, 1980, **73**, 556–561.
16 L. Jeloaica and V. Sidis, *Chem. Phys. Lett.*, 1999, **300**, 157–162.
17 X. Sha and B. Jackson, *Surf. Sci.*, 2002, **496**, 318–330.
18 Y. Ferro, F. Marinelli and A. Allouche, *J. Chem. Phys.*, 2002, **116**, 8124–8131.
19 S. Casolo, O. M. Løvvik, R. Martinazzo and G. F. Tantardini, *J. Chem. Phys.*, 2009, **130**, 054704.
20 V. V. Ivanovskaya, A. Zobelli, D. Teillet-Billy, N. Rougeau, V. Sidis and P. R. Briddon, *Eur. Phys. J. B*, 2010, **76**, 481–486.
21 L. Hornekær, E. Rauls, W. Xu, Ž. Šljivančanin, R. Otero, I. Stensgaard, E. Lægsgaard, B. Hammer and F. Besenbacher, *Phys. Rev. Lett.*, 2006, **97**, 186102.
22 T. Zecho, A. Güttler, X. Sha, D. Lemoine, B. Jackson and J. Küppers, *Chem. Phys. Lett.*, 2002, **366**, 188.
23 B. Jackson and D. Lemoine, *J. Chem. Phys.*, 2001, **114**, 474–482.
24 M. Bonfanti and R. Martinazzo, *Phys. Rev. B: Condens. Matter Mater. Phys.*, in press.
25 M. Bonfanti, B. Jackson, K. H. Hughes, I. Burghardt and R. Martinazzo, *J. Chem. Phys.*, 2015, **143**, 124704.
26 M. Agúndez, J. Goicoechea, J. Cernicharo, A. Faure and E. Roueff, *Astrophys. J.*, 2010, **713**, 662.
27 M. Bonfanti, G. F. Tantardini and R. Martinazzo, *J. Phys. Chem. A*, 2014, **118**, 6595–6603.
28 A. J. H. M. Meijer, A. J. Farebrother, D. C. Clary and A. J. Fisher, *J. Phys. Chem. A*, 2001, **105**, 2173–2182.
29 M. Rutigliano, M. Cacciatore and G. Billing, *Chem. Phys. Lett.*, 2001, **340**, 13–20.
30 S. Morisset, F. Aguillon, M. Sizun and V. Sidis, *Phys. Chem. Chem. Phys.*, 2003, **5**, 506–513.
31 S. Morisset, F. Aguillon, M. Sizun and V. Sidis, *Chem. Phys. Lett.*, 2003, **378**, 615–621.
32 R. Martinazzo and G. F. Tantardini, *J. Phys. Chem. A*, 2005, **109**, 9379–9383.
33 R. Martinazzo and G. F. Tantardini, *J. Chem. Phys.*, 2006, **124**, 124703.
34 M. Sizun, D. Bachellerie, F. Aguillon and V. Sidis, *Chem. Phys. Lett.*, 2010, **498**, 32–37.
35 M. Bonfanti, S. Casolo, G. F. Tantardini and R. Martinazzo, *Phys. Chem. Chem. Phys.*, 2011, **13**, 16680–16688.
36 S. Casolo, G. F. Tantardini and R. Martinazzo, *Proc. Natl. Acad. Sci. U. S. A.*, 2013, **110**, 6674–6677.
37 S. Casolo, G. Tantardini and R. Martinazzo, *J. Phys. Chem. A*, 2016, **120**, 5032–5040.
38 M. Pasquini, M. Bonfanti and R. Martinazzo, *Phys. Chem. Chem. Phys.*, 2016, **18**, 6607–6617.
39 A. J. Meijer, A. J. Farebrother and D. C. Clary, *J. Phys. Chem. A*, 2002, **106**, 8996–9008.
40 M. Bonfanti, B. Jackson, K. H. Hughes, I. Burghardt and R. Martinazzo, *J. Chem. Phys.*, 2015, **143**, 124703.
41 U. Weiss, *Quantum Dissipative Systems*, World Scientific, Singapore, 3rd edn, 2008.
42 R. Zwanzig, *Nonequilibrium Statistical Mechanics*, Oxford University Press, Oxford, 2001.
43 A. O. Caldeira and A. J. Leggett, *Physica A*, 1983, **121**, 587–616.
44 A. J. Leggett, *Phys. Rev. B: Condens. Matter Mater. Phys.*, 1984, **30**, 1208–1218.
45 G. W. Ford, J. T. Lewis and R. F. O'Connel, *Phys. Rev. A: At., Mol., Opt. Phys.*, 1988, **37**, 4419.
46 M. Bonfanti and R. Martinazzo, *Research Advances in Quantum Dynamics*, InTech, 2016.
47 M. Bonfanti and R. Martinazzo, *Int. J. Quantum Chem.*, 2016, **116**, 1575–1602.
48 H.-D. Meyer, U. Manthe and L. S. Cederbaum, *Chem. Phys. Lett.*, 1990, **165**, 73–78.
49 M. H. Beck, A. Jäckle, G. Worth and H.-D. Meyer, *Phys. Rep.*, 2000, **324**, 1–105.
50 *Multidimensional Quantum Dynamics: MCTDH Theory and Applications*, ed. H.-D. Meyer, F. Gatti and G. A. Worth, Wiley-VCH, Weinheim, 2009.
51 H. Wang and M. Thoss, *J. Chem. Phys.*, 2003, **119**, 1289–1299.
52 U. Manthe, *J. Chem. Phys.*, 2009, **130**, 054109.
53 O. Vendrell and H.-D. Meyer, *J. Chem. Phys.*, 2011, **134**, 044135.
54 F. Gottwald, M. Bonfanti, R. Martinazzo, S. D. Ivanov and O. Kühn, *J. Chem. Phys.*, 2016, **145**, 126101.
55 R. Martinazzo, K. Hughes and I. Burghardt, *Phys. Rev. E: Stat., Nonlinear, Soft Matter Phys.*, 2011, **84**, 030102.
56 J. Kerwin, X. Sha and B. Jackson, *J. Phys. Chem. B*, 2006, **110**, 18811–18817.
57 G. A. Worth, M. H. Beck, A. Jäckle, O. Vendrell and H.-D. Meyer, The MCTDH Package, Version 8.2, (2000). H.-D. Meyer, Version 8.3 (2002), Version 8.4 (2007). O. Vendrell and H.-D. Meyer Version 8.5 (2013). Version 8.5 contains the ML-MCTDH algorithm. Current versions: 8.4.12 and 8.5.5 (2016), see http://mctdh.uni-hd.de/.
58 S. Sakong and P. Kratzer, *J. Chem. Phys.*, 2010, **133**, 054505.
59 M. Bonfanti, M. F. Somers, C. Díaz, H. F. Busnengo and G.-J. Kroes, *Z. Phys. Chem.*, 2013, **227**, 1397–1420.
60 E. R. Latimer, F. Islam and S. D. Price, *Chem. Phys. Lett.*, 2008, **455**, 174–177.
61 R. Martinazzo, B. Vacchini, K. H. Hughes and I. Burghardt, *J. Chem. Phys.*, 2011, **134**, 011101.

